Eur. Phys. J. Spec. Top. (2024) 233:1191–1207
https://doi.org/10.1140/epjs/s11734-024-01151-0

THE EUROPEAN PHYSICAL JOURNAL SPECIAL TOPICS

Review

Investigations of nuclear isomeric states utilizing heavy-ion storage rings

Yury A. Litvinov[1,2,a] and Wolfram Korten[3,b]

[1] Atomic, Quantum and Fundamental Physics, GSI Helmholtzzentrum für Schwerionenforschung GmbH, Darmstadt 64291, Germany
[2] Helmholtz Forschungsakademie Hessen für FAIR (HFHF), GSI Helmholtzzentrum für Schwerionenforschung GmbH, Campus Darmstadt, Darmstadt 64291, Germany
[3] Nuclear Physics Division, Institute of Research into the Fundamental Laws of the Universe, CEA, Université Paris-Saclay, Gif-sur-Yvette 91191, France

Received 4 February 2024 / Accepted 13 March 2024 / Published online 10 April 2024

Abstract Heavy-ion storage rings allow for storing secondary ion beams for extended periods of time. Sophisticated beam manipulation techniques, detection capabilities and thin targets provide unique conditions for a broad range of physics experiments. In this work, the investigations related to nuclear isomeric states are reviewed.

1 Introduction

The nuclear force acting between nucleons composing atomic nuclei is highly complicated and is far from being understood. This force, which results from an interplay of strong, weak, and electromagnetic interactions, is responsible for nuclear properties like deformation, shell structure, nucleon–nucleon correlations, decay properties as well as for the rich spectra of excited states [1]. Among the latter, isomers are long-lived states, decay of which is for various reasons hindered [2, 3]. Comprehending the reasons behind such hindrances can act as a sensitive probe to constrain nuclear theory and, hence, progress toward understanding the underlying nuclear force.

The plot of all observed nuclei as a function of their proton (Z) and neutron (N) numbers is commonly called the nuclear chart. There are numerous isomeric states known on this chart spanning a large range of excitation energies, half-lives, shapes, and other quantum numbers [4]. Measurements of the properties of nuclear isomers are pursued at basically all radioactive-ion beam facilities by employing many different approaches. In this contribution, we discuss multifaceted studies of isomers conducted at heavy-ion storage rings [5].

High mass resolving power attainable in storage rings, combined with the sensitivity to detecting single particles, is the base for investigations of rarely produced isomers. By selecting the beam energy, isomers in a specific atomic charge state can be produced. Thanks to the ultra-high-vacuum (UHV) environment, the rings offer the capability of preserving this charge state for extended periods of time. This enables the possibility to study the influence of the electron configuration on the isomeric decay properties. Indeed, it is possible that the dominant decay branches in neutral atoms are completely disabled in highly charged ions or that new decay channels open up. Several investigations of the properties of the nuclear isomeric states have been conducted in storage rings, which will be reviewed in this work. Furthermore, storage rings allow for colliding stored beams with atoms, electrons or photons which will be explored in the near future also in the context of stored isomeric beams.

[a] e-mail: y.litvinov@gsi.de (corresponding author)
[b] e-mail: w.korten@cea.fr

2 Heavy-ion storage ring facilities

In the focus of this work are heavy-ion storage rings which can be employed for studies of or with nuclear isomers. The latter have to be produced elsewhere as a secondary beam with suitable parameters prior to their injection and storage in the ring [6]. Therefore, the storage rings have to be coupled to radioactive-ion beam facilities. There are presently three such combinations in the world [7], namely the FRagment Separator (FRS) [8] and the Experimental Storage Ring (ESR) [9] at GSI Helmholtz Center for Heavy Ion Research (GSI) in Germany, the Radioactive Ion Beam Line in Lanzhou 2 (RIBLL2) and the Experimental Cooler-Storage Ring (CSRe) [10] at the Institute of Modern Physics (IMP) in China, and the Superconducting Radioactive Isotope Beam Separator (BigRIPS) [11] and the Ring for Rare Radioactive Isotopes (R3) [12] at RIKEN Nishina Center for Accelerator-Based Science (RIKEN) in Japan. Whereas the GSI and IMP complexes are based on heavy-ion synchrotrons, SIS-18 and CSRm, respectively, as driver accelerators, the one at RIKEN is built upon a chain of cyclotrons. In the former case, the synchrotrons deliver primary beams as short bunches which match the injection timing of the accepting storage ring. In the case of a cyclotron, the primary beam is (quasi)continuous. The ions of interest are produced at random times which leads to the injection and storage of individual pre-identified particles [13, 14].

The isomeric states of interest are created in a violent nuclear reaction together with a swarm of other reaction products [15]. Projectile fragmentation or, in the case of uranium beam, also projectile fission reactions are employed routinely. Although these reactions are kinematically very different [16], in the present context, it is essential that the resulting momentum spread of the produced fragments is typically larger than the injection acceptance of a storage ring of about 1%. All three facilities operate at relativistic energies which facilitates stripping of bound electrons off the fragments directly in the production target [17]. By selecting dedicated stripper foils at different focal planes of a fragment separator, the charge state distributions can be further tuned [18]. The heavy-ion storage rings discussed here are high-energy machines designed to accept secondary beams with energies from a few 10 to several 100 MeV/u.

All particles within the magnetic rigidity, $B\rho$, acceptance of the fragment separator and the ring are transmitted and injected together with the isomers of interest. The magnetic rigidity is defined as $B\rho = p/q$, with the ion momentum $p = mv\gamma$, charge state q, mass m, velocity v, and the relativistic Lorentz factor γ. Employing energy degraders in a fragment separator introduces Z-dependent energy losses, $\Delta E \propto Z^2$ [8]. Although this additional separation criterion can be used to prepare pure mono-isotopic beams, mono-isomeric beams cannot be separated in flight [19].

The majority of the discussed here experiments have been conducted at the ESR and very first results were obtained at the CSRe. Dedicated studies involving nuclear isomers yet to be accomplished at the R3. If not stated differently, the assumed machine in the following discussion will be the ESR.

A storage ring is an accelerator structure composed of drift sections and dipole, quadrupole, and sextupole magnets, as well as higher-order correction elements. A scheme of the 108 m long ESR is shown in Fig. 1, where various, though far from all, components are indicated. These components will be discussed in the following sections. As can be seen in the figure, the drift sections are densely packed with various accelerator and experimental equipment.

The ESR is a versatile machine with a rich inventory of beam manipulations. Important to mention for the outlook section is that the ESR is capable to decelerate secondary beams and extract them either toward HITRAP [21] or to a dedicated low-energy storage ring CRYRING [20].

3 Storage ring mass spectrometry and its limitations

The orbit length, C, of a particle in a storage ring depends only on its magnetic rigidity. It is, therefore, straightforward that, since all different nuclear species injected and stored simultaneously in the ring have the same $B\rho$, they will be indistinguishable neither by their revolution frequencies nor by their orbits.

The key for studies of isomeric states is the ability to separate them from the inevitable contaminants and especially from the corresponding ground states and to identify them unambiguously. It can be shown [32] that the relative difference of revolution frequencies, $\Delta f/f$, or the revolution times, $\Delta T/T$, of stored particles with the relative difference of mass-to-charge ratios, $\Delta(m/q)/(m/q)$, is given by the relation:

$$\frac{\Delta f}{f} = -\frac{\Delta T}{T} = -\frac{1}{\gamma_t^2}\frac{\Delta(m/q)}{m/q} + \frac{\Delta v}{v}\left(1 - \frac{\gamma^2}{\gamma_t^2}\right), \tag{1}$$

where γ_t, dubbed transition energy, is a parameter defined by the ion optics of the ring. It is directly connected to the momentum compaction factor $\alpha_p = 1/\gamma_t^2$, which quantifies the relative change of the orbit length $\Delta C/C$ induced by a relative change of magnetic rigidity $\Delta B\rho/B\rho$. This is the basic equation of the storage ring mass

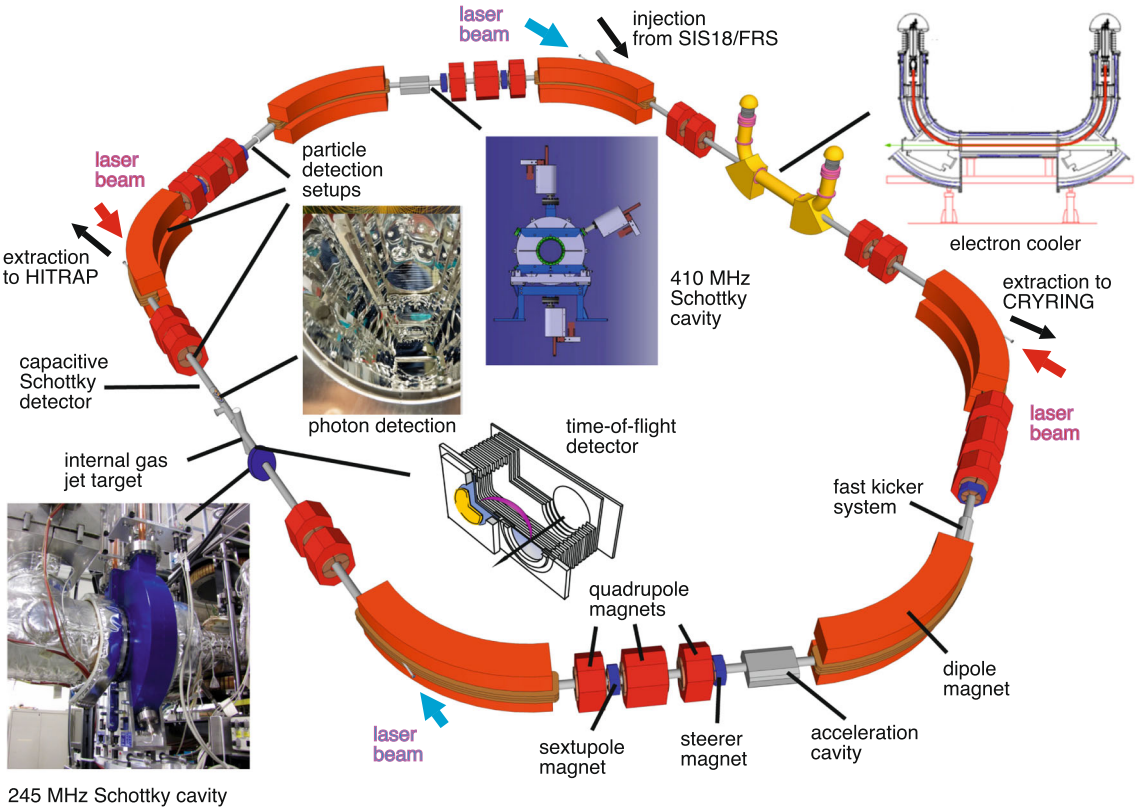

Fig. 1 Schematic illustration of the experimental storage ring ESR at GSI [9]. The ESR has a circumference of 108 m. The dipole, quadrupole and sextupole as well as kicker and steerer magnets are shown. Furthermore, correction coils are integrated into the dipoles. The ions can be injected from the fragment separator FRS or directly from the synchrotron SIS-18. The maximum magnetic rigidity of the ESR is 10 Tm. The heart of the ESR is the electron cooler. The interaction length of the electron and ion beams is 2.5 m. The diameter of the electron beam is $\sim$ 5 cm. The cooler is routinely operated up to ion energies of 420 MeV/u. The stochastic cooling (not shown) operates at a fixed velocity of the ions corresponding to 400 MeV/u. The revolution frequency of an ion beam at 400 MeV/u is about 2 MHz. The acceleration cavity is employed to alter the energy of the stored beams. In the last years it is mostly used to decelerate the beams for either experiments directly in the ESR or for their extraction toward low-energy machines CRYRING@ESR [20] or HITRAP [21]. The lowermost energy achieved in the ESR for experiments with cooled beams is about 5 MeV/u [22, 23]. A stored beam can be brought into collisions with gas atoms/molecules from the dedicated ultra-thin, windowless gas target [24, 25]. Co- and/or counter-propagating laser beams can be coupled to the ring, which is equipped with a dedicated optical detection unit [26, 27]. The velocity of electrons in the electron cooler can be quickly modified by an integrated drift tube setup, thus introducing a co-propagating electron target with a well-defined energy difference to the ion beam [28]. The time-of-flight detector [29] is composed of a foil (light blue) and a set of micro-channel plates (yellow). The guiding of secondary electrons, released from the foil due to crossing it ions, is done by perpendicularly arranged electrostatic field, created by the shown electrodes, and a weak magnetic field, created by Helmhotz coils placed outside of vacuum pipe. The locations of the three employed non-destructive Schottky detectors (capacitive, 245 MHz [30] and 410 MHz [31]) are indicated. Since the principles of the 245 and 410 MHz detectors are very similar, a photograph and a scheme are depicted. More details can be found in Ref. [5]. Photographs: S. Sanjari and R. Sanchez, GSI, Darmstadt

spectrometry (SRMS). The principles of the SRMS and results are exhaustively reviewed in the literature [33–37] and especially its use to study radioactive decays of highly charged ions [38–41]. Here, we briefly discuss its application to experiments related to nuclear isomers.

The term containing the velocity spread, $\Delta v/v$, on the right-hand side of Eq. (1) determines the mass resolving power and, thus, needs to be reduced as much as possible. There are two approaches to minimize it.

The first one is to decrease the large velocity spread of the injected secondary beams by beam cooling [42, 43]. In the electron cooler device, see Fig. 1, the circulating beam is merged over a length of a few meters with a continuous beam of electrons. For our applications, the latter can be considered as mono-energetic. The electrons are accelerated to the desired velocity prior to merging them with the ion beam. The ions circulate in the ring with revolution frequencies of a few hundred kHz to a few MHz. At every turn, they interact with fresh electrons. After multiple passages through the cooler, they are finally forced to the same velocity as the electrons. The transverse

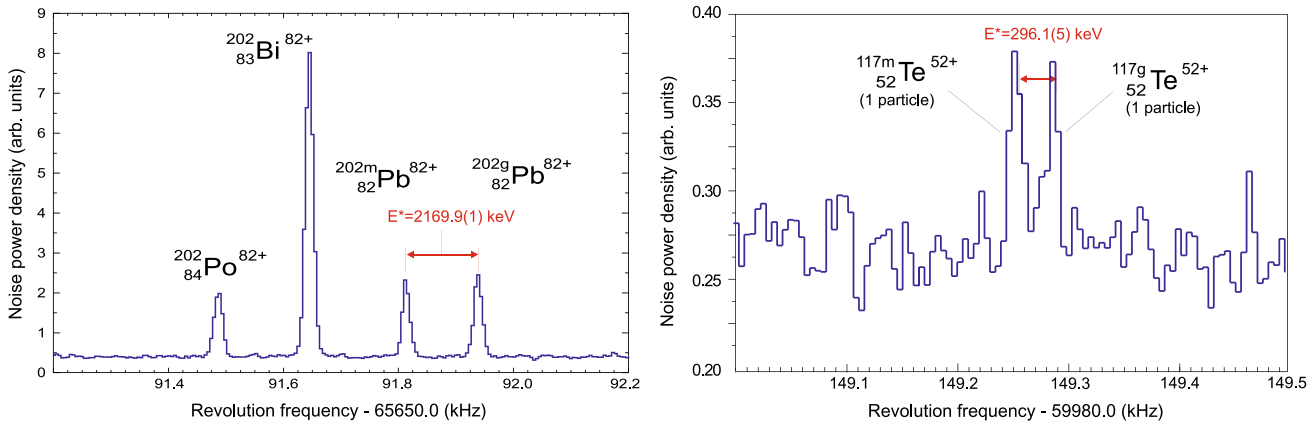

Fig. 2 Isomeric states of fully ionized $^{202m}Pb^{82+}$ (Left) and $^{117m}Te^{52+}$ (Right) well resolved from the corresponding ground states. The isomers were produced through fragmentation of ^{209}Bi projectiles. Both spectra were taken in the ESR with the capacitive Schottky detector and averaged for 30 s. The intensity of the peaks is proportional to the number of composing them ions. The ground and isomeric states of $^{117}Te^{52+}$ are represented by a single ion each. The isomer excitation energies (E^*) are taken from Ref. [56]. The figures are modified from Ref. [55]

size of the electron beam is a few cm which allows the cooling of all ion species stored in the ring independent of their m/q values. The efficiency of the electron cooling critically depends on the velocity difference between the ions and the electrons [44]. Note that to have the same $B\rho = mv\gamma/q$, nuclear species with different m/q must have the corresponding different v. For hot beams, the cooling process can take from a few seconds up to several minutes. Therefore, only relatively long-lived isomeric states can be studied by applying the electron cooling alone.

By utilizing the stochastic pre-cooling [45], it is feasible to quickly reduce the initial velocity spread to about 10^{-4} [46]. In such case the subsequent electron cooling efficiently cools the beam within about a second. The overall stochastic and electron cooling process can be optimized to last only a few seconds [47–49]. The stochastic cooling cools ions only in a limited range of m/q values and effectively heats the species with m/q values other than in this range. This combined cooling has been implemented to the measurement of the bound-state beta decay of $^{207}Tl^{81+}$ ions [50], see Sect. 4.

In the context of the application of the electron cooling to studies of isomeric states, two important issues need to be emphasized. The highly charged ions are in an equilibrium between the focusing electron cooling force and de-focusing interactions of the beam ions among themselves. Therefore, the final velocity spread depends on the number of ions of a particular ion species, though not on the total number of the stored ions. For low intensities of below $\sim 10^3$ ions, the mean longitudinal spacing between the ions increases to a couple of cm and the intra-beam interactions are disabled [51]. One speaks of building a crystalline beam [52–54], where the ions are traveling one behind the other on the same mean orbit. The velocity spread of such a crystalline beam is as small as $\Delta v/v \approx 10^{-7}$ leading to the mass resolving power approaching $m/\Delta m = 10^6$. Examples of well-resolved ground and isomeric states of fully ionized $^{202}Pb^{82+}$ and $^{117}Te^{52+}$ [55] ions coasting in the ring are shown in Fig. 2.

This $m/\Delta m$ could just be sufficient to resolve an isomeric state with an excitation energy of $E^* = \Delta m = 100$ keV from a ground state of a nucleus with mass $m \approx 100$ GeV. However, the highly charged ions in the ground and isomeric state are coasting with the same velocities on orbits which are a few μm apart. Therefore, the ion on a shorter orbit has—at some point—to overtake the ion on the longer orbit, which, however, cannot happen since the highly charged ions repel from each other. As a result, the ion on a shorter orbit will effectively be slowed down and the one on the longer orbit will be accelerated, such that two ions revolve as a cluster with the same frequency. Taken the high revolution frequencies in the ring, such blocking cannot be avoided. The illustration of the blocking effect is shown in Fig. 3 [55].

Hence, independent of the high mass resolving power, there is a limit on the lowest isomer excitation energy which can directly be resolved from the corresponding ground state. This limit is not present when only one particle is stored, which has to belong either to the ground or to the isomeric state [57]. After many injections into the ring, sometimes it is feasible to obtain spectra of single particles representing both states. One such example is shown in Fig. 4.

The second approach to minimize the term containing the velocity spread in Eq. (1) is to employ the isochronous ion-optical setting of the storage ring. In this mode, a faster and a slower particles of the same ion species move on the respectively longer and shorter orbits such that their revolution frequencies are (in the first order) the same. This operation mode is very similar to the recently developed multi-reflection time-of-flight spectrometers (MR-TOF) [58, 59], if one imagines the arcs of the ring acting as magnetic mirrors instead of the electrostatic ones in the MR-TOFs. The isochronous condition requires that $\gamma = \gamma_t$. This type of SRMS is called Isochronous Mass

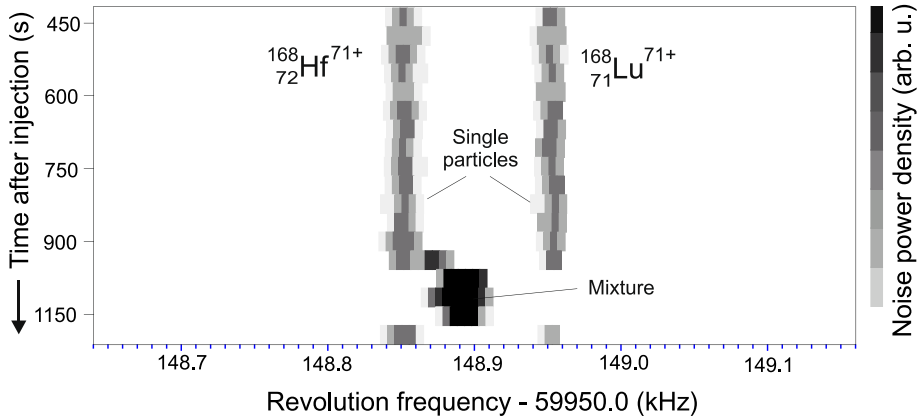

Fig. 3 Schottky frequency spectra versus time after injection into the ESR. Data were acquired with the capacitive Schottky detector. Each spectrum was averaged for 30 s. Traces of the hydrogen-like $^{168}Hf^{71+}$ and fully ionized $^{168}Lu^{71+}$ ions are represented by a single particle each. The m/q difference between these isobars is $\Delta(m/q) \approx 2.6 \cdot 10^{-5}$. The Schottky noise power is proportional to q^2. The region indicated as "mixture" is about a factor of 4 more intense than the mean intensity of individual single ions with $q = 71+$. This indicates that for about 90 s the Schottky detector observed a cluster of 2 particles with a total charge $2 \cdot 71+$. This observation is interpreted as a Coulomb blocking between these ions, see text. This is an example with an untypically large $\Delta(m/q)$. In the case of unperturbed peaks of single ions $^{117m}Te^{52+}$ and $^{117g}Te^{52+}$, shown in Fig. 2, the corresponding $\Delta(m/q) \approx 6.5 \cdot 10^{-6}$, that is 2 times smaller. The figure is modified from Ref. [55]

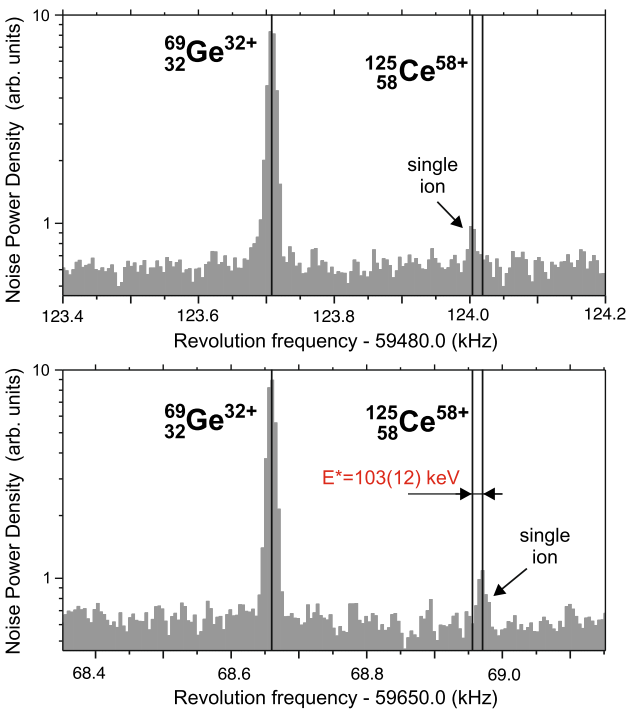

Fig. 4 Schottky frequency spectra of single particles representing the isomeric state (Top) and the ground state (Bottom) of the fully ionized $^{125}Ce^{58+}$ ions. The peak of the fully ionized $^{69}Ge^{32}$ ions is shown as a frequency reference. In the majority of measured spectra, the two states of $^{125}Ce^{58+}$ ions were present as "mixtures" (see Fig. 3). The resolving of these states became possible only when ions of only one kind were present. The obtained difference in frequency corresponds to the reported excitation energy of $E^* = 103(12)$ keV. The figure is modified from Ref. [57]

Spectrometry (IMS) [60–65]. Since the $B\rho$ injection acceptance is small, nuclides in a limited range of m/q values will be isochronous. This range is commonly called isochronous window, in which the mass resolving power can approach $m/\Delta m = 2 \cdot 10^5$ [66–68]. Outside of this window $\gamma \neq \gamma_t$ and $m/\Delta m$ deteriorates rapidly. This is depicted for non-isochronous ^{24}Al ions in the left panel of Fig. 5, where the projection shows the corresponding revolution time spectrum. Although the attainable mass resolving power is somewhat smaller than for the electron-cooled beams, the main advantage of this approach is that no cooling at all is needed, thus providing access to the much shorter-lived nuclear species. Furthermore, the mass resolving power can be increased as well as the deterioration can be avoided if the momentum spread of the ions is reduced either directly in the ring or in the fragment separator [69], though this is achieved at the cost of the reduced transmission efficiency. Another advantage of IMS is that stored particles are moving on distinct orbits and no Coulomb blocking is possible.

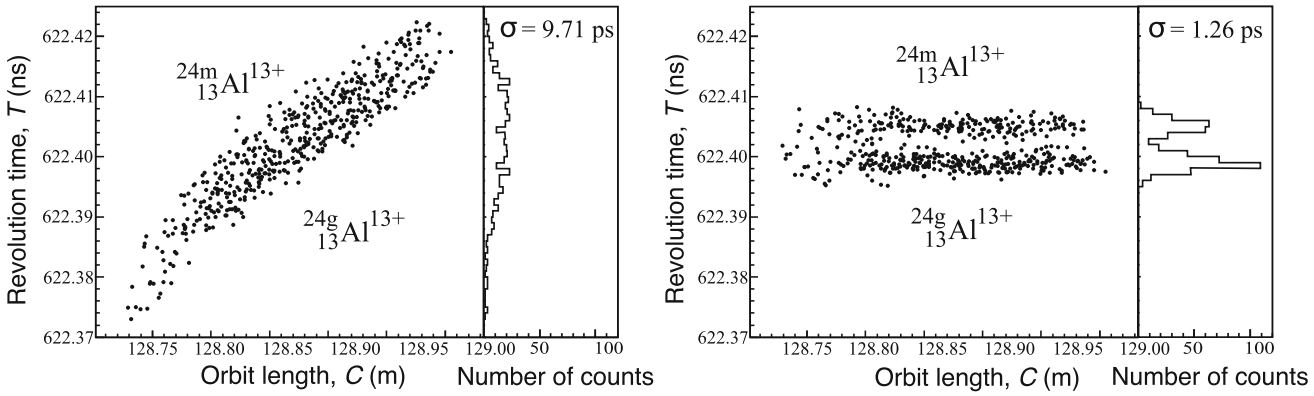

Fig. 5 Revolution times (T) as a function of orbit length (C) measured for fully ionized $^{24}Al^{13+}$ ions at the CSRe. If a single time-of-flight (ToF) detector is used, only the revolution times can be measured yielding the projected spectrum in the left panel. Installing a second ToF detector adds in-ring velocity, v, measurement of every ion and, hence, its orbit length via $C = T \cdot v$. The combined information on T and v allows for correction of the non-isochronicity as shown in the right panel, where the ground and isomeric states of $^{24}Al^{13+}$ are clearly resolved. The employed correction is the basis of the $B\rho$-IMS technique [70, 71]. The figures are modified from Ref. [71]

The resolving power of IMS can be boosted dramatically if the velocity of every stored ion is measured in addition to its revolution frequency (time) [72]. This has been realized in the CSRe, which enabled one to correct for the non-isochronicity effects, see the right panel in Fig. 5 [70, 71, 73].

4 Time-resolved revolution frequency measurement

According to Eq. (1), to deduce the m/q values of the stored ions, which is in first place needed for particle identification, their revolution frequencies need to be measured. Several nuclear species with known masses are required to calibrate the acquired frequency spectrum according to Eq. (1). In the context of the isomeric states, the measured frequency allows a direct determination of the corresponding excitation energies, E^*. Another important quantity is the lifetime of the isomeric state, which can be addressed by monitoring the intensity changes of the corresponding frequency peaks. Due to the change of the mass in the decay, the latter is manifested by a sudden change of the revolution frequency of the decayed ion.

The ultimate goal is to measure the frequency of every single stored ion. A straightforward way to achieve this is to use (semi)destructive detectors. Dedicated ultra-thin foil-based detectors have been developed [29, 74], where the one used in the ESR is indicated in Fig. 1 as time-of-flight (ToF) detector. A self-supporting, a few $\mu g/cm^2$ thick carbon foil is installed directly into the UHV of the ring. The circulating ions punch through it at every revolution causing the release of secondary electrons from its surface. These electrons are guided to a set of micro-channel plate detectors which give precise timing stamps. After assigning the corresponding time stamps to each individual particle, the determination of the revolution frequency is relatively straightforward [75–77]. All particles are detected and, since the ion-optical transmissions for the ground and isomeric states of the same nuclear species is the same, by counting the number of the observed particles in both states, the isomeric ratios can be determined. The interactions of the ions with the foil lead to their inevitable losses from the ring after at maximum a few hundred revolutions. Therefore, the application of such detectors for lifetime determination is limited to the μs range. Two examples of half-life measurements are shown in Fig. 6.

Ideally, the measurement of the revolution frequencies should be non-destructive, which is achieved with Schottky noise spectroscopy [81]. The first generation of the Schottky detector employed in the ESR has a pair of copper electrodes placed inside the ring aperture parallel to each other above and below the beam [82]. Another pair of electrodes arranged on the sides of the beam is not relevant in the present discussion. This device is indicated as the capacitive Schottky detector in Fig. 1. At a typical energy of about 400 MeV/u, the revolution frequencies in the ESR are about 2 MHz. The circulating highly charged ions induce an electric current on the surface of the conducting vacuum pipe as well as on the Schottky detector electrodes. The noise from the electrodes is electronically processed and then Fourier transformed. The frequencies around 30$^{\text{th}}$ harmonic of the revolution frequency, that is around 60 MHz, are analyzed. The disadvantage of this Schottky detector is its relatively low signal-to-noise characteristics: To measure the frequency of a single ion with charge $q \sim 60$, averaging of Fourier transformed spectra for several ten seconds is required. The examples of individual Schottky frequency spectra are shown, e.g., in Figs. 2, 3, and 4, where the offset frequency of about 60 MHz is subtracted. The noise power

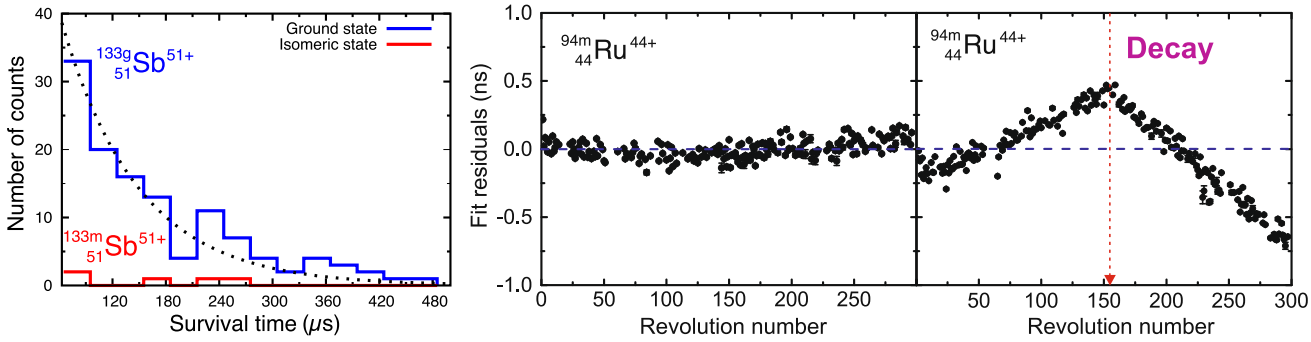

Fig. 6 (Left) Estimation of an upper limit of the half-life of the fully ionized $^{133m}Sb^{51+}$ isomer [78]. Measurements were done with the (semi)destructive time-of-flight (ToF) detector in the ESR. This $J^\pi = (21/2^+)$ isomer has a half-life of $T_{1/2} = 16.54(19)$ μs in the neutral atom [79]. Ions surviving for more than 200 μs can be seen. The surviving probability of the isomer turned out to be compatible with the one obtained for the ions in the ground state. The figure is taken from Ref. [78]. (Right) Decay of single fully ionized $^{94m}Ru^{44+}$ isomers in the CSRe [80]. Precise timing signals were acquired with the ToF detector and were fitted as a function of the revolution number. Two panels depict residuals of the data points from the fit function, which show dramatically different patterns. In the second one, at about 150th revolution a sudden change in the ion mass is observed, whereas no such features are seen in the first panel. From 49 measured decay events, a half-life $T_{1/2} = 102(17)$ μs was determined for the 8^+ isomeric state in $^{94}Ru^{44+}$. The figures are taken from Ref. [80]

of a peak in the spectrum is directly proportional to the number of composing this peak ions and to their charge squared. By creating consecutive in time Schottky spectra, the simultaneous monitoring of the development of particle intensities for various nuclear species can be done, which is the basis for half-life as well as branching ratio measurements. If the daughter particle remains in the storage ring acceptance, a correlation in time of the reduction/increase of the intensity of the peak of the parent/daughter ions can be observed. The described technique is called time-resolved Schottky Mass Spectrometry (SMS) [83]. All SMS measurements reported here were conducted in the ESR. Conventionally, SMS is applied on the cooled ion beams.

To boost the signal-to-noise characteristics of the Schottky detectors, instead of capacitive arrangement of the electrodes, a pill-box cavity has been employed. The passing by ions lose tiny amounts of energy which is sensed through a loop coupler. The cavity has its fundamental resonant frequency which defines the harmonic of the ion's revolution frequency to be studied. Two generations of such detectors have been developed which are resonant at 245 MHz [30] and 410 MHz [31], respectively. Both detectors enable frequency determination of a single particle with charge $q \sim 30$ within about 10 ms. In all SMS measurements discussed here, except for the most recent investigations of ^{72}Ge and ^{205}Tl, the capacitive Schottky detector has been used.

5 Experimental results

5.1 Basic properties of nuclear isomers

SRMS is routinely employed to measure unknown masses of exotic nuclei far from stability [36, 37]. One of the primary aims in such measurements is to cover a large region of the nuclear chart in the same experiment. In this way, the masses are determined with the same method and thus with same systematic errors. Furthermore, a large number of references masses, which are used for a robust calibration in Eq. 1, are included. Generally, it is expected that all isomeric states which can be produced in the chosen nuclear reaction should be present in the measured revolution frequency spectra. Here, one has to consider the shortest lifetimes and minimal mass resolving power that are required for different detection approaches as discussed above. Indeed, numerous known nuclear isomers have been observed in several mass measurement campaigns at GSI and IMP.

Often, the exact excitation energy of the isomer is not known and is then determined through direct mass measurements. One such example is ^{52}Co, for which the masses of both, the isomeric and ground, states have been measured with IMS at IMP [65]. The $J^\pi = 2^+$, $T_{1/2} = 104(11)$ ms isomeric state at $E^* = 387(13)$ keV was previously observed in β-decay of ^{52}Ni but its position relative to the ground state was unknown. In another example, the excitation energy $E^* = 4560(100)$ keV was measured with IMS in the ESR for the $J^\pi = (21/2^+)$ isomer in ^{133}Sb, see Fig. 6 (Left), contributing an important ingredient to construct the level scheme in this nucleus [78], which is just one proton away from the doubly magic ^{132}Sn.

By combining the data from different SMS and IMS experiments conducted at GSI and IMP on the production of high-spin ($J^\pi = 19/2^-$) isomers in the mirror nuclei ^{53}Fe and ^{53}Co, the dependence of the isomeric ratios on the

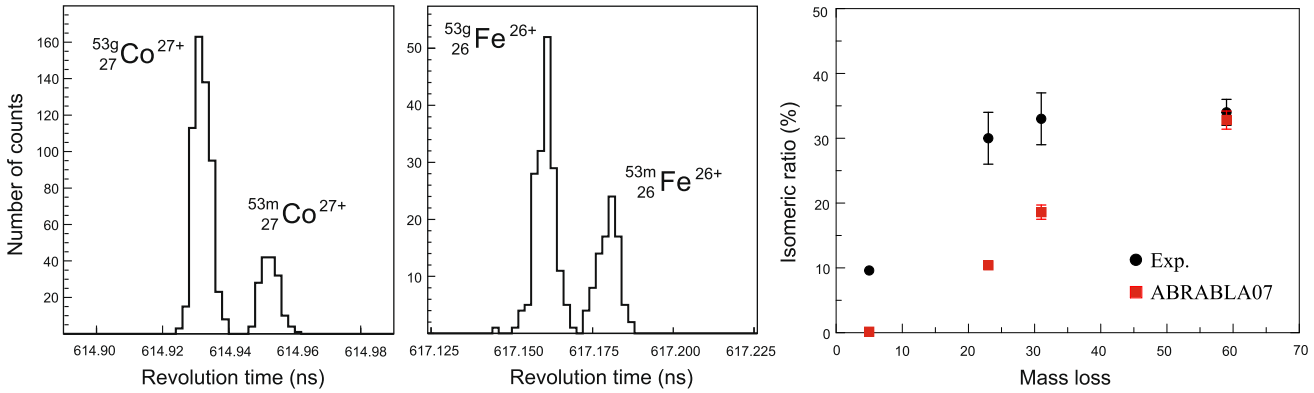

Fig. 7 (Left) Revolution time spectra of the ground and isomeric states of fully ionized $^{53}Co^{27+}$ and $^{53}Fe^{26+}$ ions. The spectra were acquired with IMS at IMP. (Right) Isomeric ratio for the production of $J^{\pi} = 19/2^{-}$ isomers as a function of the mass loss, which is the measure of the number of nucleons removed from the projectile. The theoretical calculations were done with the ABRABLA parametrization [85]. The figures are taken from Ref. [84]

projectile mass could be investigated [84]. Figure 7 illustrates the measured spectra of the well-resolved ^{53m}Fe and ^{53m}Co isomers as well as the deduced isomeric ratios as a function of the mass loss, which quantifies the number of nucleons that are removed from the projectile to produce the isomer. The obtained isomeric ratios grow rapidly with increasing mass loss and then remain about constant. The data are compared to the calculations performed with the ABRABLA parametrization [85].

Apart from the known isomeric states, observations of new isomers cannot be excluded. In the ESR experiment studying ^{152}Sm projectile fragments with SMS, a new isomeric state in ^{125}Ce [57] was seen, which is shown in Fig. 4. The excitation energy of $E^* = 103(12)$ keV has been determined from a single fully ionized ion, which was stored in the ESR for $t = 193(1)$ s. Several new isotopes [86] and isomers [87] have been observed in SMS measurements of neutron-rich heavy ^{238}U projectile fragments in the ESR. Among the new isomers were ^{234m}Ac, ^{234n}Ac, ^{228m}Ac, ^{228m}Fr, ^{214m}Bi, and ^{213m}Bi [87]. The second isomer ^{212n}Bi was observed in the same experiment and later was investigated in more detail [88]. The obtained excitation energy of $E^* = 1478(30)$ keV agrees well with the theoretical calculations but is significantly lower than the previously accepted value of $E^* > 1910$ keV. By applying the IMS technique at IMP, a new isomeric state in neutron-deficient ^{101}In was discovered at an excitation energy of $E^* = 659(50)$ keV [89, 132]. A subsequent complementary measurement with Penning-trap mass spectrometry [90], confirmed the IMP result and extended the data on In isomers further up to ^{99}In [91], which could be used to test ab initio calculations in this region as well as to constrain the mass of doubly magic ^{100}Sn derived from β-decay spectroscopy [92, 93].

In addition to serendipitous discoveries of new isomeric states described above, of special importance are dedicated searches of specific isomers. SRMS with its sensitivity to detection of individual stored ions turned out to be a powerful tool to look for extremely rarely produced long-lived isomers. Projectile fragmentation of ^{197}Au has been employed to search for isomers in the neutron-rich Hf-Os region. By utilizing SMS in the ESR, isomeric states in ^{183,184,186}Hf, ^{186,187}Ta,^{186}W, ^{190,192,194}Re, and ^{195}Os have been observed [94–96]. These investigations have facilitated the design of dedicated spectroscopic studies of some of the isomers at the KISS facility in RIKEN [97–99].

5.2 Decays of isomers in highly charged ions

The observation of new isomers and the measurement of their excitation energies can in principle be accomplished with other experimental methods. Storage rings are important machines to address the decay properties of the isomers in high atomic charge states. The decay probabilities and channels known in neutron atoms can be altered significantly once all or most of the bound electrons are removed.

A straightforward example is internal conversion (IC) which is simply disabled in the absence of bound electrons. Hence, the half-life of the isomers will be significantly increased. Studies of the decay of fully ionized isomers were among the first experiments in the ESR [100]. Figure 8 illustrates the Schottky spectra of ground and isomeric states of fully ionized $^{149}Dy^{66+}$ ions measured later in the ESR [101], which was addressed together with the isomers in ^{151}Er and ^{144}Tb. In the neutral atom, the ^{149m}Dy isomeric state decays to 99.3% via IC giving a half-life $T_{1/2}^{\text{neutral}} = 0.49(2)$ s [79]. This half-life is too short for the electron cooling and the isomer would not be seen in the ESR by applying the conventional SMS. However, the disabled IC branch increases the half-life by a factor of 22(2) to $T_{1/2} = 11(1)$ s. This measurement can in turn be used to determine the conversion coefficient which

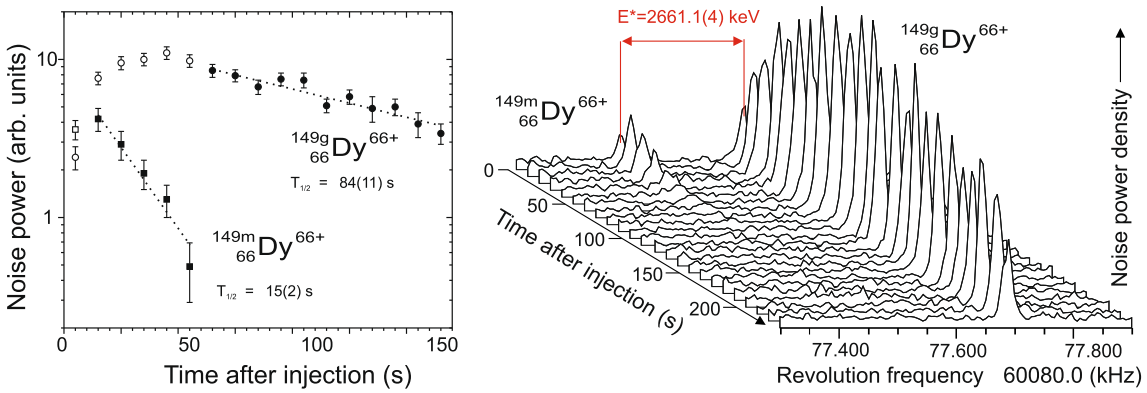

Fig. 8 (Left) Decay curves of fully ionized ^{149}Dy^{66+} ions in the ground and isomeric states measured with SMS in the ESR [101]. The half-life values are given in the laboratory frame and have to be corrected by the Lorentz factor of the relativistic ions. (Right) The noise power density spectra of one injection into the ESR illustrating the decay of these states. It shall be noted that the decay of the isomer populates the ground state and that ions in both states experience losses due to recombination in the electron cooler and collisions with rest gas atoms. The isomer excitation energy (E^*) is taken from Ref. [56]. The figures are modified from Ref. [101]

amounts to $\alpha_{\mathrm{tot}} = 27.3$. Another similar example is illustrated in Fig. 2, where the atomic half-life of ^{117m}Te is $T_{1/2}^{\mathrm{neutral}} = 103(3)$ ms [79].

Figure 9 presents the half-life measurement of the $J^\pi = 11/2^-$ isomeric state in fully ionized neutron-rich ^{207}Tl^{81+}. This is the example where the combined stochastic pre-cooling and electron cooling have been utilized [102], see Sect. 3. The obtained half-life $T_{1/2} = 1.49(11)$ s agrees well with the expected prolongation due to disabling the internal conversion channel. Such half-life extensions due the disabled IC channel have been measured for many fully ionized isomeric states with both IMS and SMS. In addition to the excitation energies also the corresponding lifetimes have been measured for the majority of the isomers mentioned in Sect. 5.1. A summary of the measured half-lives of highly charged ions, including isomeric states can be found in a recent Ref. [41].

A special case of a half-life measurement of fully ionized isomers is the $J^\pi = 0^+ \rightarrow J^\pi = 0^+$ transition. If the 0^+ state is the first excited state and if its excitation energy is below the electron–positron pair-creation threshold $E^* < 1022$ keV, then, due to angular momentum conservation, it can only decay by a two-photon emission or by a particle emission. Although such measurements at the ESR have been discussed since several decades, the expected half-lives are in the ms range, which could not be approached with conventional SRMS methods. By utilizing the recently developed resonant Schottky cavities, the de-excitation of the first 0^+ state ($E^* = 691$ keV) in fully ionized ^{72}Ge^{32+} ions has been successfully studied [103]. Especially the highest signal-to-noise characteristics of the 410 MHz detector turned out to be decisive. To avoid the lengthy cooling, the ring was tuned into the isochronous mode. Herewith, a novel method of Schottky + Isochronous Mass Spectrometry (S+IMS) has been implemented. It is noted that S+IMS technique was previously shown to work on long-lived

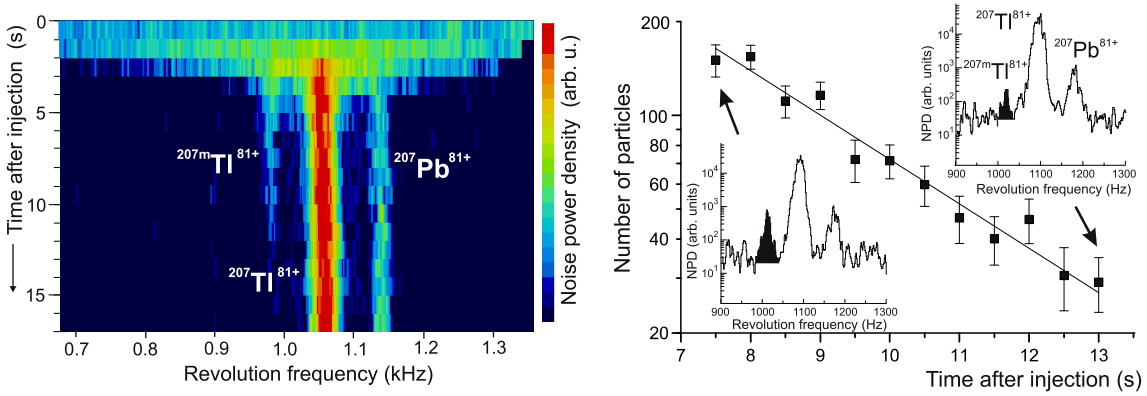

Fig. 9 (Left) Schottky frequency spectra of $A = 207$, $q = 81+$ isobars measured in the ESR. Combined stochastic and electron cooling methods accelerate the overall cooling process to below 5 s [46]. (Right) The decay curve of the fully ionized ^{207}Tl^{81+} isomers. The inserts show the noise power density at the beginning and at the end of the measurement. The figure is modified from Ref. [50]

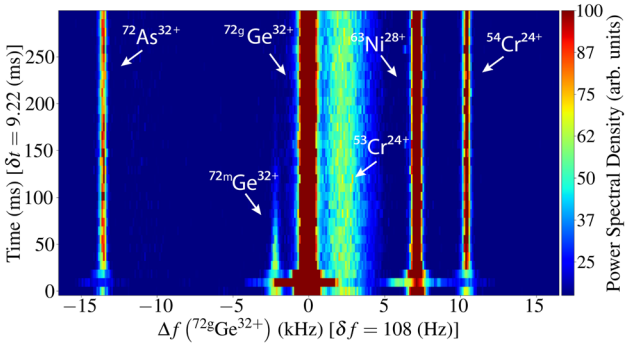

Fig. 10 Schottky frequency spectra of the fully ionized $^{72}Ge^{32+}$ ions stored in the ESR [103]. The ESR is tuned into the isochronous ion-optical mode. Data were taken with the Schottky detector resonant at 410 MHz [31]. Employing Schottky noise spectroscopy in this mode enabled the combined Schottky + Isochronous Mass Spectrometry (S+IMS). Shown is a sum of 102 individual injections into the ESR. The decay of the $^{72m}Ge^{32+}$ is clearly observed. This trace corresponds to the first excited 0^+ state in ^{72}Ge. Consequently, the main decay channel to the $J^\pi = 0^+$ ground state is 2γ emission. The figure is taken from [103]

species at the ESR [104] and the CSRe [105]. To enhance the mass resolving power, the momentum spread of the stored ions has been significantly reduced by in-ring mechanical scrapers. A sum of 102 individual injections into the ESR is shown in Fig. 10. The measured probability of 2γ decay in $^{72}Ge^{32+}$ is about a factor of 10 larger than expected, which remains to be explained theoretically [103].

The only half-life prolongation in hydrogen-like ion is published for $^{192m}Os^{75+}$ [106]. The measured lifetime $\tau = 15.1^{+1.5}_{-1.3}$ s is in agreement with the expected $\tau = 13.0(24)$ s calculated from the known lifetime of neutral atoms and IC branching ratio.

In addition to electromagnetic decays described above, important results have been obtained for weak transitions. The first excited state ($J^\pi = 1/2^-$, $E^* = 2.329(7)$ keV) in ^{205}Pb atoms [79] decays within a few ten μs to the ground state. Due to the such short half-life, it is practically impossible to directly measure the weak decay of this state. However, the decay to the ground state of ^{205}Tl is important for astrophysical applications as this can be the main path to deplete ^{205}Pb in hot stellar environments [107]. To address the weak matrix element of this transition, the rate of the bound-state beta decay [108, 109] of fully ionized $^{205}Tl^{81+}$ has been measured in the ESR by applying SMS and the detector resonant at 245 MHz. $^{205}Tl^{81+}$ decays predominantly to the excited state of interest. The obtained transition matrix element will be utilized to infer the weak decay of the short-lived excited state in ^{205}Pb. The corresponding results are yet unpublished. A similar measurement has been conducted with fully ionized $^{187}Re^{75+}$ which decays by bound-state beta decay to the first excited state ($J^\pi = 1/2^-$, $T_{1/2} = 2.38(18)$ ns, $E^* = 9.756(19)$ keV) in ^{187}Os [110].

6 Isomeric beams

By employing the $B\rho - \Delta E - B\rho$ separation method in a fragment separator it is possible to produce a pure mono-isotopic beam [19]. Although it is presently impossible to prepare in flight mono-isomeric beams, there are ways to prepare those in a storage ring. A trivial approach can be used, when either the ground or the isomeric states are much shorter lived than the respective other state. Then, after an appropriate waiting time, one can achieve a clean beam. In cases where the excitation energy is large enough, a mechanical scraping of one of the states can be attempted, see Fig. 11. In a test experiment, scraping of one from two electron-cooled ion species separated by a mass difference of $Q_{EC} = 3388$ keV was shown [19]. Although no pure isomeric beam has been prepared in a storage ring so far, this measurement shows the feasibility of such production at least for isomers with excitation energies exceeding 3.4 MeV.

Figure 12 depicts results of the experiment addressing di-electronic recombination (DR) on lithium-like $^{234}Pa^{88+}$ ions in the ESR [111]. DR is a resonant process in which the recombination is accompanied by the excitation of one of the bound electrons without X-ray emission [112]. The energy of the electrons is tuned by ramping the drift tubes in the electron cooler. The energy can be scanned very accurately to measure the DR resonances. The left panel of Fig. 12 displays the rate of $^{234}U^{89+}$ ions in a particle detector intercepting the inner orbits in the ESR. Due to a significant difference of the half-lives of the ground and isomeric states of ^{234}Pa, see the insert in the left panel, these ions are mainly attributed to the β^- decay of the isomeric state $^{234m}Pa^{88+}$. The DR resonances were measured shortly after the injection of the beam, when both states of ^{234}Pa were present, and then 5 min

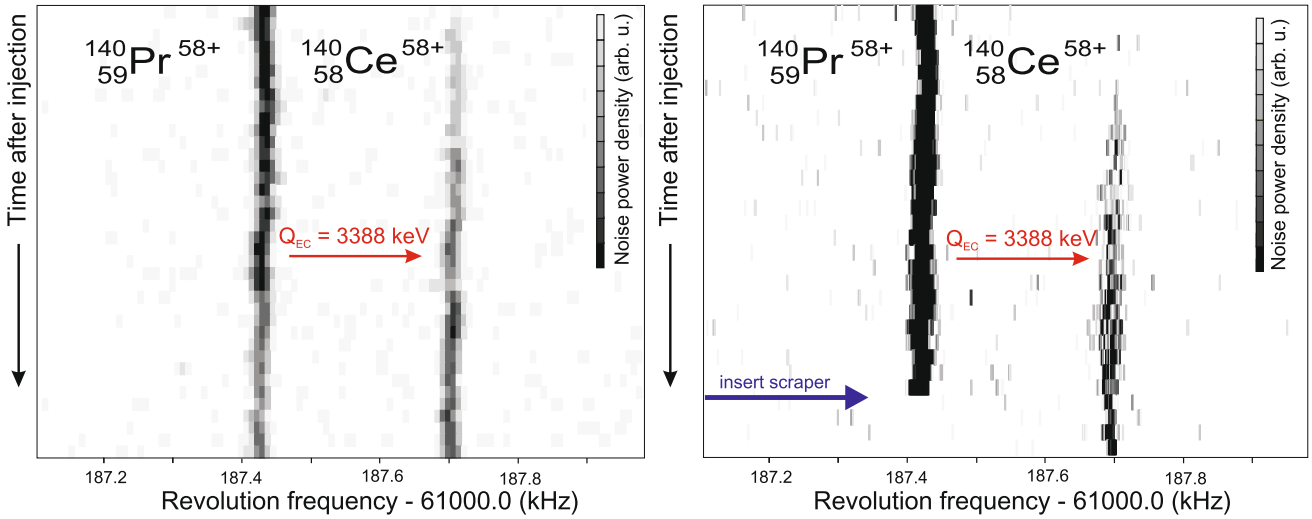

Fig. 11 Schottky frequency spectra of stored in the ESR hydrogen-like $^{140}Pr^{58+}$ and fully ionized $^{140}Ce^{58+}$ ions [47]. The separation in mass between these two isobars corresponds to $Q_{EC} = 3388$ keV. The undisturbed measurement is shown in the left panel. A mechanical scraper was inserted to remove ions of one isobar as shown in the right panel. The figure is modified from Ref. [19]

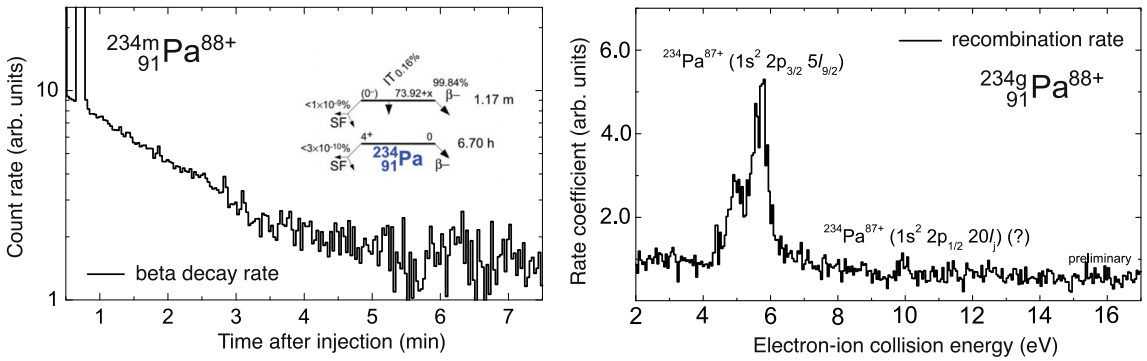

Fig. 12 (Left) The rate of $^{234}U^{89+}$ ions in a particle detector in the ESR. These ions were produced in beta decay of the stored $^{234}Pa^{88+}$ ions [111]. The insert shows the partial decay scheme of the isomeric and ground states of ^{234}Pa [79]. Since the half-life of the isomeric state is significantly shorter than the one of the ground state, the detected ions are mainly attributed to the decay of the isomeric state $^{234m}Pa^{88+}$. The decay rate reflects directly the intensity of the stored $^{234m}Pa^{88+}$ ions. (Right) Dielectronic recombination resonances measured 5 min after the injection of $^{234}Pa^{88+}$ beam into the ESR, when the isomeric state has completely decayed. The figures are modified from Ref. [111]

later, when the isomeric state fully decayed. The DR resonances of the ground state are shown in the right panel of Fig. 12. Since the DR is a recombination process, the charge is altered and, thus, also the orbit. By blocking the corresponding orbits, all down-charged ions can be removed from the ring. Hence, by tuning on the correct resonance, the DR can be used as a tool to deplete one of the states. It is important to note that the non-resonant radiative recombination will contribute to charge changing reactions for both states.

7 Conclusion and outlook

This work is a brief review of experimental techniques employed in heavy-ion storage rings for investigations of properties of nuclear isomeric states. The presented characteristic results show the breadth and power of this research. Campaigns for large-scale mass measurements will continue in the future at the ESR, CSRe and R3, which will undoubtedly contribute with new data (excitation energies, half-lives, isomeric ratios, production cross sections) on already known isomers as well as new isomers will be found.

Recently, a new, dedicated low-energy storage ring CRYRING has been installed behind the ESR at GSI [20]. The beams decelerated in the ESR can be transported to the CRYRING@ESR. The advantage of CRYRING is an even better vacuum and the possibility to decelerate the beams to lower energies, where the low limit is determined by beam lifetime in the ring. Another facility connected to the ESR is HITRAP [21]. In HITRAP, the beams extracted from the ESR at 4 MeV/u are decelerated in several steps to be finally stored as highly charged ions in an ion trap. These new facilities open new opportunities for investigations with nuclear isomers.

With the establishment of the combined S+IMS technique, dedicated investigations of rare decay modes of isomeric states will be intensified. First of all, 2γ decay probabilities of other low-energy $0^+ \rightarrow 0^+$ transitions will be measured, e.g., in ^{98}Mo and ^{98}Zr nuclei. Above an excitation energy of $E^* = 1022$ keV, competing to 2γ de-excitation is the decay by positron-electron pair creation. A unique ion is $^{194}Pb^{82+}$ where the sum of the K-shell electron binding energy ($BE \sim 101$ keV) and the excitation energy of the first excited 0^+ state $E^* \sim 931$ keV [79] is slightly above the pair creation threshold. If such a decay can be observed, the electron will occupy the empty K-shell and a monochromatic positron will be emitted to the continuum [113].

Nuclear Excitation by Electron Capture (NEEC) is an illusive decay process which has been proposed in the 1970s [114]. A successful observation of NEEC has been reported in Ref. [115], which has been later disputed in the literature [116, 117]. A heavy-ion storage ring has been considered since a long time as an ideal machine for such measurements [118]. Several approaches are being pursued, where the electrons of the cooler or the bound atomic electrons in the internal gas jet are considered in various experimental proposals. One of the ways to identify NEEC is to detect high-energy γ-rays from a high-energy isomeric state, which is excited to an intermediate state via NEEC. The isomeric state in ^{93}Mo is ($J^\pi = 21/2^+$, $T_{1/2} = 6.85$ h, $E^* = 2425$ keV [79]) is often considered for this purpose [119]. Another proposed example is the isomer in ^{129}Sb ($J^\pi = (19/2^-)$, $T_{1/2} = 17.7(1)$ h, $E^* = 1851$ keV [79]) which has a $(15/2^-)$ state only 10 keV above it. An isomeric beam of fully ionized $^{129}Sb^{51+}$ can be prepared in the ESR, transmitted to CRYRING, where it can be further decelerated down to very low energies to eliminate possible background due to Coulomb excitation. Afterward the low-energy beam can be extracted and implanted in a foil, which will be the source of electrons to be captured onto ^{129m}Sb. The detection of a 1128 keV γ-ray would manifest the NEEC process [20].

Since recently, nuclear reaction studies of astrophysical relevance are being intensively conducted at the ESR. In these experiments, a stored, decelerated, cooled beam is brought into collisions with a hydrogen gas jet to measure cross sections of proton-induced reactions [22, 23, 120]. In the future, it is planned to address also other types of reactions in the ESR. Furthermore, various reactions experiments are planned at the CRYRING@ESR [121]. Often, individual reaction cross sections on the ground and on the isomeric states are important. Here, the inventory of methods to determine isomeric ratios can be applied to obtain the composition of the beam of interest.

Of special interest is the isomeric state in ^{229}Th which has the lowest known excitation energy of about only 8 eV [122]. One of the exciting motivations to study this isomer is its potential application as a robust—insensitive to external perturbations—highly precise frequency standard. A heavy-ion storage ring is a facility where a cooled beam of fully ionized $^{229}Th^{90+}$ ions can be uniquely prepared. The possibility to couple lasers to the ring, see Fig. 1, offers the capability for a direct laser excitation of the isomeric state. Furthermore, modifications of isomeric decay properties due to hyperfine interaction in highly charged ions can be studied [123].

In summary, the present research into nuclear isomers as well as the plans for future experiments show exciting prospects and have a high discovery potential. In addition to the presently running storage rings, new facilities will become operational soon [124]. In a few years, the High Intensity Accelerator Facility (HIAF) will be completed in Huizhou in China [125]. Its core is a new spectrometer storage ring (SRing) connected via a new high-acceptance fragment separator to a 35-Tm synchrotron. Several new storage rings are planned at the Facility for Ion and Antiproton Research (FAIR) [126, 127], though the time of their realization is presently uncertain. An advantage of having a dedicated low-energy storage ring at an ISOL facility has been thoroughly investigated [128]. The construction of such a machine is strongly supported by the community, as reflected in the latest NuPECC Long Range Plan [129], but the project still awaits its approval. Last but not least, the quest for measuring neutron-induced reactions, as considered by coupling a storage ring to a free-neutron target [130, 131], is being approached by several groups. Studies of nuclear isomers or application of isomeric beams will inevitably play an important role at these future facilities.

Acknowledgements This contribution would not be possible without successful collaboration with colleagues working at the ESR, CSRe, and R3. This research received support from the European Research Council (ERC) under the EU Horizon 2020 research and innovation program (ERC-CoG "ASTRUm"), the State of Hesse within the Research Cluster ELEMENTS (Project ID 500/10.006), and the French-German Exchange Program at GSI (IN2P3-CEA/IRFU-GSI) (Project ID 21.87).

Funding Open Access funding enabled and organized by Projekt DEAL.

References

1. A. Bohr, B.R. Mottelson, *Nuclear Structure* (World Scientific Publishing Company, Singapore, New Jersey, London, HongKong, 1998)
2. P. Walker, G. Dracoulis, Energy traps in atomic nuclei. Nature **399**, 35–40 (1999). https://doi.org/10.1038/19911
3. P. Walker, Z. Podolyák, 100 years of nuclear isomers-then and now. Phys. Scr. **95**, 044004 (2020). https://doi.org/10.1088/1402-4896/ab635d
4. S. Garg, B. Maheshwari, B. Singh et al., Atlas of nuclear isomers–second edition. At. Data Nucl. Data Tables **150**, 101546 (2023). https://doi.org/10.1016/j.adt.2022.101546
5. M. Steck, Y.A. Litvinov, Heavy-ion storage rings and their use in precision experiments with highly charged ions. Prog. Part. Nucl. Phys. **115**, 103811 (2020). https://doi.org/10.1016/j.ppnp.2020.103811
6. H. Geissel, K. Beckert, F. Bosch et al., First storage and cooling of secondary heavy-ion beams at relativistic energies. Phys. Rev. Lett. **68**, 3412–3415 (1992). https://doi.org/10.1103/PhysRevLett.68.3412
7. Y.A. Litvinov, S. Bishop, K. Blaum et al., Nuclear physics experiments with ion storage rings. Nucl. Instrum. Methods B **317**, 603–616 (2013). https://doi.org/10.1016/j.nimb.2013.07.025
8. H. Geissel, P. Armbruster, K.H. Behr et al., The GSI projectile fragment separator (FRS): a versatile magnetic system for relativistic heavy ions. Nucl. Instrum. Methods B **70**, 286–297 (1992). https://doi.org/10.1016/0168-583X(92)95944-M
9. B. Franzke, The heavy ion storage and cooler ring project ESR at GSI. Nucl. Instrum. Methods B **24–25**, 18–25 (1987). https://doi.org/10.1016/0168-583X(87)90583-0
10. J.W. Xia, W.L. Zhan, B.W. Wei et al., The heavy ion cooler-storage-ring project (HIRFL-CSR) at Lanzhou. Nucl. Instrum. Methods A **488**, 11–25 (2002). https://doi.org/10.1016/S0168-9002(02)00475-8
11. T. Kubo, D. Kameda, H. Suzuki et al., BigRIPS separator and zero degree spectrometer at RIKEN RI beam factory. Prog. Theor. Exp. Phys. **2012**, 03–003 (2012). https://doi.org/10.1093/ptep/pts064
12. A. Ozawa, T. Uesaka, M. Wakasugi, Rare-RI ring collaboration: the rare-RI ring. Prog. Theor. Exp. Phys. **2012**, 03–009 (2012). https://doi.org/10.1093/ptep/pts060
13. T. Yamaguchi, Y. Yamaguchi, A. Ozawa, The challenge of precision mass measurements of short-lived exotic nuclei: development of a new storage ring mass spectrometry. Int. J. Mass Spectrom. **349–350**, 240–246 (2013). https://doi.org/10.1016/j.ijms.2013.04.027
14. H.F. Li, S. Naimi, T.M. Sprouse et al., First application of mass measurements with the rare-RI ring reveals the solar r-process abundance trend at $A = 122$ and $A = 123$. Phys. Rev. Lett. **128**, 152701 (2022). https://doi.org/10.1103/PhysRevLett.128.152701
15. H. Geissel, G. Münzenberg, K. Riisager, Secondary exotic nuclear beams. Ann. Rev. Nucl. Part. Sci. **45**, 163–203 (1995). https://doi.org/10.1146/annurev.ns.45.120195.001115
16. C.A. Bertulani, P. Danielewicz, *Introduction to Nuclear Reactions* (CRC Press, Boca Raton, 2021)
17. C. Scheidenberger, T. Stöhlker, W.E. Meyerhof et al., Charge states of relativistic heavy ions in matter. Nucl. Instrum. Methods B **142**, 441–462 (1998). https://doi.org/10.1016/S0168-583X(98)00244-4
18. N. Winckler, H. Geissel, Y.A. Litvinov et al., Orbital electron capture decay of hydrogen- and helium-like ^{142}Pm ions. Phys. Lett. B **679**, 36–40 (2009). https://doi.org/10.1016/j.physletb.2009.07.019
19. C. Scheidenberger, K. Beckert, P. Beller et al., Isobar separation at FRS-ESR—a development towards pure isomeric stored beams. Hyperfine Interact. **173**, 61 (2006). https://doi.org/10.1007/s10751-007-9543-2
20. M. Lestinsky, V. Andrianov, B. Aurand et al., Physics book: CRYRING@ESR. Eur. Phys. J. Spec. Top. **225**, 797–882 (2016). https://doi.org/10.1140/epjst/e2016-02643-6
21. F. Herfurth, Z. Andelkovic, W. Barth et al., The HITRAP facility for slow highly charged ions. Phys. Scr. **T166**, 014065 (2015). https://doi.org/10.1088/0031-8949/2015/t166/014065
22. J. Glorius, C. Langer, Z. Slavkovská et al., Approaching the Gamow window with stored ions: direct measurement of ^{124}Xe(p, γ) in the ESR storage ring. Phys. Rev. Lett. **122**, 092701 (2019). https://doi.org/10.1103/PhysRevLett.122.092701
23. J. Glorius, C.G. Bruno, Low-energy nuclear reactions with stored ions: a new era of astrophysical experiments at heavy ion storage rings. Eur. Phys. J. A **59**, 81 (2023). https://doi.org/10.1140/epja/s10050-023-00985-x
24. M. Kühnel, N. Petridis, D.F.A. Winters et al., Low-internal target from a cryogenically cooled liquid microjet source. Nucl. Instrum. Methods A **602**, 311–314 (2009). https://doi.org/10.1016/j.nima.2008.12.212
25. K. Grigoryev, Internal targets at storage rings. Phys. Scr. **T166**, 014050 (2015). https://doi.org/10.1088/0031-8949/2015/t166/014050
26. W. Nörtershäuser, R. Sánchez, Laser spectroscopy at storage rings. Phys. Scr. **T166**, 014020 (2015). https://doi.org/10.1088/0031-8949/2015/T166/014020

27. J. Ullmann, Z. Andelkovic, C. Brandau et al., High precision hyperfine measurements in bismuth challenge bound-state strong-field QED. Nat. Commun. **8**, 15484 (2017). https://doi.org/10.1038/ncomms15484
28. C. Brandau, C. Kozhuharov, Z. Harman et al., Isotope shift in the dielectronic recombination of three-electron $^{A}Nd^{57+}$. Phys. Rev. Lett. **100**, 073201 (2008). https://doi.org/10.1103/PhysRevLett.100.073201
29. J. Trötscher, K. Balog, H. Eickhoff, Mass measurements of exotic nuclei at the ESR. Nucl. Instrum. Methods B **70**, 455–458 (1992). https://doi.org/10.1016/0168-583X(92)95965-T
30. F. Nolden, P. Hülsmann, Y.A. Litvinov et al., A fast and sensitive resonant Schottky pick-up for heavy ion storage rings. Nucl. Instrum. Methods A **659**, 69–77 (2011). https://doi.org/10.1016/j.nima.2011.06.058
31. M.S. Sanjari, D. Dmytriiev, Y.A. Litvinov et al., A 410 MHz resonant cavity pickup for heavy ion storage rings. Rev. Sci. Instr. **91**, 083303 (2020). https://doi.org/10.1063/5.0009094
32. B. Franzke, H. Geissel, G. Münzenberg, Mass and lifetime measurements of exotic nuclei in storage rings. Mass Spectr. Rev. **27**, 428–469 (2008). https://doi.org/10.1002/mas.20173
33. F. Bosch, H. Geissel, Y.A. Litvinov et al., Experiments with stored exotic nuclei at relativistic energies. Int. J. Mass Spectrom. **251**, 212–219 (2006). https://doi.org/10.1016/j.ijms.2006.01.037
34. F. Bosch, Y.A. Litvinov, T. Stöhlker, Nuclear physics with unstable ions at storage rings. Prog. Part. Nucl. Phys. **73**, 84–140 (2013). https://doi.org/10.1016/j.ppnp.2013.07.002
35. F. Bosch, Y.A. Litvinov, Mass and lifetime measurements at the experimental storage ring of GSI. Int. J. Mass Spectrom. **349–350**, 151–161 (2013). https://doi.org/10.1016/j.ijms.2013.04.025
36. Y.H. Zhang, Y.A. Litvinov, T. Uesaka, H.S. Xu, Storage ring mass spectrometry for nuclear structure and astrophysics research. Phys. Scr. **91**, 073002 (2016). https://doi.org/10.1088/0031-8949/91/7/073002
37. T. Yamaguchi, H. Koura, Y.A. Litvinov, M. Wang, Masses of exotic nuclei. Prog. Part. Nucl. Phys. **120**, 103882 (2021). https://doi.org/10.1016/j.ppnp.2021.103882
38. Y.A. Litvinov, F. Bosch, Beta decay of highly charged ions. Rep. Prog. Phys. **74**, 016301 (2011). https://doi.org/10.1088/0034-4885/74/1/016301
39. Y.A. Litvinov, F. Bosch, C. Kozhuharov et al., At the borderline between atomic and nuclear physics: two-body β-decay of highly charged ions. Phys. Scr. **T144**, 014001 (2011). https://doi.org/10.1088/0031-8949/2011/T144/014001
40. D. Atanasov, K. Blaum, F. Bosch et al., Between atomic and nuclear physics: radioactive decays of highly-charged ions. J. Phys. B **48**, 144024 (2015). https://doi.org/10.1088/0953-4075/48/14/144024
41. Y.A. Litvinov, R.J. Chen, Radioactive decays of stored highly charged ions. Eur. Phys. J. A **59**, 102 (2023). https://doi.org/10.1140/epja/s10050-023-00978-w
42. H. Poth, electron cooling: theory, experiment, application. Phys. Rep. **196**, 135–297 (1990). https://doi.org/10.1016/0370-1573(90)90040-9
43. I.N. Meshkov, Electron cooling: status and perspectives. Phys. Element. Part. At. Nuclei **25**, 631–661 (1994)
44. M. Steck, P. Beller, K. Beckert et al., Electron cooling experiments at the ESR. Nucl. Instrum. Methods A **532**, 357–365 (2004). https://doi.org/10.1016/j.nima.2004.06.065
45. D. Möhl, G. Petrucci, L. Thorndahl, S. van der Meer, Physics and technique of stochastic cooling. Phys. Rep. **58**, 73–102 (1980). https://doi.org/10.1016/0370-1573(80)90140-4
46. F. Nolden, K. Beckert, P. Beller et al., Experience and prospects of stochastic cooling of radioactive beams at GSI. Nucl. Instrum. Methods A **532**, 329–334 (2004). https://doi.org/10.1016/j.nima.2004.06.062
47. Y.A. Litvinov, F. Bosch, N. Winckler et al., Observation of non-exponential orbital electron capture decays of hydrogen-like ^{140}Pr and ^{142}Pm ions. Phys. Lett. B **664**, 162–168 (2008). https://doi.org/10.1016/j.physletb.2008.04.062
48. P. Kienle, F. Bosch, P. Bühler et al., High-resolution measurement of the time-modulated orbital electron capture and of the β^+ decay of hydrogen-like $^{142}Pm^{60+}$ ions. Phys. Lett. B **726**, 638–645 (2013). https://doi.org/10.1016/j.physletb.2013.09.033
49. F.C. Ozturk, B. Akkus, D. Atanasov et al., New test of modulated electron capture decay of hydrogen-like ^{142}Pm ions: precision measurement of purely exponential decay. Phys. Lett. B **797**, 134800 (2019). https://doi.org/10.1016/j.physletb.2019.134800
50. H. Geissel, Y.A. Litvinov, F. Attallah et al., New results with stored exotic nuclei at relativistic energies. Nucl. Phys. A **746**, 150–155 (2004). https://doi.org/10.1016/j.nuclphysa.2004.09.030
51. M. Steck, K. Beckert, H. Eickhoff et al., Anomalous temperature reduction of electron-cooled heavy ion beams in the storage ring ESR. Phys. Rev. Lett. **77**, 3803–3806 (1996). https://doi.org/10.1103/PhysRevLett.77.3803
52. J.P. Schiffer, P. Kienle, Could there be an ordered condensed state in beams of fully stripped heavy ions? Z. Phys. A **321**, 181 (1985). https://doi.org/10.1007/BF01411964
53. T. Schätz, U. Schramm, D. Habs, Crystalline ion beams. Nature **412**, 717–720 (2001). https://doi.org/10.1038/35089045
54. T. Shirai, M. Ikegami, S. Fujimoto et al., One-dimensional beam ordering of protons in a storage ring. Phys. Rev. Lett. **98**, 204801 (2007). https://doi.org/10.1103/PhysRevLett.98.204801
55. Y.A. Litvinov, H. Geissel, T. Radon et al., Mass measurement of cooled neutron-deficient bismuth projectile fragments with time-resolved Schottky mass spectrometry at the FRS-ESR facility. Nucl. Phys. A **756**, 3–38 (2005). https://doi.org/10.1016/j.nuclphysa.2005.03.015
56. F.G. Kondev, M. Wang, W.J. Huang et al., The NUBASE2020 evaluation of nuclear physics properties. Chinese Phys. C **45**, 030001 (2021). https://doi.org/10.1088/1674-1137/abddae

57. B. Sun, Y.A. Litvinov, P.M. Walker et al., Discovery of a new long-lived isomeric state in ^{125}Ce. Eur. Phys. J. A **31**, 393–394 (2007). https://doi.org/10.1140/epja/i2006-10252-0
58. H. Wollnik, History of mass measurements in time-of-flight mass analyzers. Int. J. Mass Spectrom. **349–350**, 38–46 (2013). https://doi.org/10.1016/j.ijms.2013.04.023
59. R.N. Wolf, F. Wienholtz, D. Atanasov, ISOLTRAP's multi-reflection time-of-flight mass separator/spectrometer. Int. J. Mass Spectrom. **349–350**, 123–133 (2013). https://doi.org/10.1016/j.ijms.2013.03.020
60. M. Hausmann, F. Attallah, K. Beckert et al., First isochronous mass spectrometry at the experimental storage ring ESR. Nucl. Instrum. Methods A **446**, 569–580 (2000). https://doi.org/10.1016/S0168-9002(99)01192-4
61. M. Hausmann, J. Stadlmann, F. Attallah et al., Isochronous mass measurements of hot exotic nuclei. Hyperfine Interact. **132**, 289–295 (2001). https://doi.org/10.1023/A:1011911720453
62. J. Stadlmann, M. Hausmann, F. Attallah et al., Direct mass measurement of bare short-lived ^{44}V, ^{48}Mn, ^{41}Ti and ^{45}Cr ions with isochronous mass spectrometry. Phys. Lett. B **586**, 27–33 (2004). https://doi.org/10.1016/j.physletb.2004.02.014
63. X.L. Yan, H.S. Xu, Y.A. Litvinov et al., Mass measurement of ^{45}Cr and its impact on the Ca-Sc cycle in x-ray bursts. Astrophs. J. **766**, 8 (2013). https://doi.org/10.1088/2041-8205/766/1/l8
64. Y.H. Zhang, H.S. Xu, Y.A. Litvinov et al., Mass measurements of the neutron-deficient ^{41}Ti, ^{45}Cr, ^{49}Fe, and ^{53}Ni nuclides: first test of the isobaric multiplet mass equation in fp-shell nuclei. Phys. Rev. Lett. **109**, 102501 (2012). https://doi.org/10.1103/PhysRevLett.109.102501
65. X. Xu, P. Zhang, P. Shuai et al., Identification of the lowest $T = 2$, $J^{\pi} = 0^{+}$ isobaric analog state in ^{52}Co and its impact on the understanding of β-decay properties of ^{52}Ni. Phys. Rev. Lett. **117**, 182503 (2016). https://doi.org/10.1103/PhysRevLett.117.182503
66. B. Sun, R. Knöbel, Y.A. Litvinov et al., Nuclear structure studies of short-lived neutron-rich nuclei with the novel large-scale isochronous mass spectrometry at the FRS-ESR facility. Nucl. Phys. A **812**, 1–12 (2008). https://doi.org/10.1016/j.nuclphysa.2008.08.013
67. X.L. Tu, H.S. Xu, M. Wang et al., Direct mass measurements of short-lived $A = 2Z - 1$ nuclides ^{63}Ge, ^{65}As, ^{67}Se, and ^{71}Kr and their impact on nucleosynthesis in the rp process. Phys. Rev. Lett. **106**, 112501 (2011). https://doi.org/10.1103/PhysRevLett.106.112501
68. Y.H. Zhang, P. Zhang, X.H. Zhou et al., Isochronous mass measurements of $T_z = -1 4 pt 0 ex fp$-shell nuclei from projectile fragmentation of ^{58}Ni. Phys. Rev. C **98**, 014319 (2018). https://doi.org/10.1103/PhysRevC.98.014319
69. H. Geissel, R. Knöbel, Y.A. Litvinov et al., A new experimental approach for isochronous mass measurements of short-lived exotic nuclei with the FRS-ESR facility. Hyperfine Interact. **173**, 49–54 (2006). https://doi.org/10.1007/s10751-007-9541-4
70. M. Wang, M. Zhang, X. Zhou et al., Bρ-defined isochronous mass spectrometry: an approach for high-precision mass measurements of short-lived nuclei. Phys. Rev. C **106**, 051301 (2022). https://doi.org/10.1103/PhysRevC.106.L051301
71. M. Zhang, X. Zhou, M. Wang et al., Bρ-defined isochronous mass spectrometry and mass measurements of ^{58}Ni fragments. Eur. Phys. J. A **59**, 27 (2023). https://doi.org/10.1140/epja/s10050-023-00928-6
72. H. Geissel, Y.A. Litvinov, Precision experiments with relativistic exotic nuclei at GSI. J. Phys. G **31**, 1779–1783 (2005). https://doi.org/10.1088/0954-3899/31/10/072
73. X. Zhou, M. Wang, Y.H. Zhang et al., Mass measurements show slowdown of rapid proton capture process at waiting-point nucleus ^{64}Ge. Nat. Phys. **19**, 1091–1097 (2023). https://doi.org/10.1038/s41567-023-02034-2
74. B. Mei, X. Tu, M. Wang et al., A high performance time-of-flight detector applied to isochronous mass measurement at CSRe. Nucl. Instrum. Methods A **624**, 109–113 (2010). https://doi.org/10.1016/j.nima.2010.09.001
75. X.L. Tu, M. Wang, Y.A. Litvinov et al., Precision isochronous mass measurements at the storage ring CSRe in Lanzhou. Nucl. Instrum. Methods A **654**, 213–218 (2011). https://doi.org/10.1016/j.nima.2011.07.018
76. P. Shuai, H.S. Xu, X.L. Tu et al., Charge and frequency resolved isochronous mass spectrometry and the mass of ^{51}Co. Phys. Lett. B **735**, 327–331 (2014). https://doi.org/10.1016/j.physletb.2014.06.046
77. Y.M. Xing, Y.H. Zhang, M. Wang et al., Particle identification and revolution time corrections for the isochronous mass spectrometry in storage rings. Nucl. Instrum. Methods A **941**, 162331 (2019). https://doi.org/10.1016/j.nima.2019.06.072
78. B. Sun, R. Knöbel, H. Geissel et al., Direct measurement of the 4.6 MeV isomer in stored bare ^{133}Sb ions. Phys. Lett. B **688**, 294–297 (2010). https://doi.org/10.1016/j.physletb.2010.04.020
79. National Nuclear Data Center. https://www.nndc.bnl.gov
80. Q. Zeng, M. Wang, X.H. Zhou et al., Half-life measurement of short-lived $^{94m}_{44}$Ru^{44+} using isochronous mass spectrometry. Phys. Rev. C **96**, 031303 (2017). https://doi.org/10.1103/PhysRevC.96.031303
81. J. Borer, P. Bramham, H.G. Hereward, et al. Non-destructive diagnostics of coasting beams with Schottky noise. in *Proc., IXth Int. Conf. on High Energy Accelerators*, SLAC, Stanford, 2–7 May 1974, pp. 53–56 (1974)
82. U. Schaaf, Schottky-Diagnose und BTF-Messungen an Gekühlten Strahlen im Schwerionenspeicherring ESR. PhD thesis, Univerisity of Frankfurt (1991)
83. Y.A. Litvinov, H. Geissel, Y.N. Novikov et al., Precision experiments with time-resolved Schottky mass spectrometry. Nucl. Phys. A **734**, 473–476 (2004). https://doi.org/10.1016/j.nuclphysa.2004.01.089
84. X.L. Tu, A. Kelić-Heil, Y.A. Litvinov et al., Application of isochronous mass spectrometry for the study of angular momentum population in projectile fragmentation reactions. Phys. Rev. C **95**, 014610 (2017). https://doi.org/10.1103/PhysRevC.95.014610

85. J.-J. Gaimard, K.-H. Schmidt, A reexamination of the abrasion–ablation model for the description of the nuclear fragmentation reaction. Nucl. Phys. A **531**, 709–745 (1991). https://doi.org/10.1016/0375-9474(91)90748-U
86. L. Chen, W.R. Plass, H. Geissel et al., Discovery and investigation of heavy neutron-rich isotopes with time-resolved Schottky spectrometry in the element range from thallium to actinium. Phys. Lett. B **691**, 234–237 (2010). https://doi.org/10.1016/j.physletb.2010.05.078
87. L.X. Chen, Investigation of stored neutron-rich nuclides in the element range of Pt–U with the FRS-ESR facility at 360–400 MeV/u. PhD thesis, University of Giessen (2008)
88. L. Chen, P.M. Walker, H. Geissel et al., Direct observation of long-lived isomers in ^{212}Bi. Phys. Rev. Lett. **110**, 122502 (2013). https://doi.org/10.1103/PhysRevLett.110.122502
89. J. Liu, Y. Zhang, Y. Xing et al., First observation of the low-lying isomer state of ^{101}In. Nucl. Phys. Rev. **35**, 439–444 (2018). https://doi.org/10.11804/NuclPhysRev.35.04.439
90. K. Blaum, High-accuracy mass spectrometry with stored ions. Phys. Rep. **425**, 1–78 (2006). https://doi.org/10.1016/j.physrep.2005.10.011
91. M. Mougeot, D. Atanasov, J. Karthein et al., Mass measurements of $^{99-101}$In challenge ab initio nuclear theory of the nuclide ^{100}Sn. Nat. Phys. **17**, 1099–1103 (2021). https://doi.org/10.1038/s41567-021-01326-9
92. C.B. Hinke, M. Böhmer, P. Boutachkov et al., Superallowed Gamow-Teller decay of the doubly magic nucleus ^{100}Sn. Nature **486**, 341–345 (2012). https://doi.org/10.1038/nature11116
93. D. Lubos, J. Park, T. Faestermann et al., Improved value for the Gamow–Teller strength of the ^{100}Sn beta decay. Phys. Rev. Lett. **122**, 222502 (2019). https://doi.org/10.1103/PhysRevLett.122.222502
94. M.W. Reed, I.J. Cullen, P.M. Walker et al., Discovery of highly excited long-lived isomers in neutron-rich hafnium and tantalum isotopes through direct mass measurements. Phys. Rev. Lett. **105**, 172501 (2010). https://doi.org/10.1103/PhysRevLett.105.172501
95. M.W. Reed, P.M. Walker, I.J. Cullen et al., Technique for resolving low-lying isomers in the experimental storage ring (ESR) and the occurrence of an isomeric state in^{192}Re. J. Phys. Conf. Ser. **381**, 012058 (2012). https://doi.org/10.1088/1742-6596/381/1/012058
96. M.W. Reed, P.M. Walker, I.J. Cullen et al., Long-lived isomers in neutron-rich $Z = 72 - 76$ nuclides. Phys. Rev. C **86**, 054321 (2012). https://doi.org/10.1103/PhysRevC.86.054321
97. P.M. Walker, Y. Hirayama, G.J. Lane et al., Properties of ^{187}Ta revealed through isomeric decay. Phys. Rev. Lett. **125**, 192505 (2020). https://doi.org/10.1103/PhysRevLett.125.192505
98. Y.X. Watanabe, P.M. Walker, Y. Hirayama et al., First direct observation of isomeric decay in neutron-rich odd-odd ^{186}Ta. Phys. Rev. C **104**, 024330 (2021). https://doi.org/10.1103/PhysRevC.104.024330
99. M. Mukai, Y. Hirayama, Y.X. Watanabe et al., Ground-state β-decay spectroscopy of ^{187}Ta. Phys. Rev. C **105**, 034331 (2022). https://doi.org/10.1103/PhysRevC.105.034331
100. H. Irnich, H. Geissel, F. Nolden et al., Half-life measurements of bare, mass-resolved isomers in a storage-cooler ring. Phys. Rev. Lett. **75**, 4182–4185 (1995). https://doi.org/10.1103/PhysRevLett.75.4182
101. Y.A. Litvinov, F. Attallah, K. Beckert et al., Observation of a dramatic hindrance of the nuclear decay of isomeric states for fully ionized atoms. Phys. Lett. B **573**, 80–85 (2003). https://doi.org/10.1016/j.physletb.2003.08.077
102. T. Ohtsubo, F. Bosch, H. Geissel et al., Simultaneous measurement of β^- decay to bound and continuum electron states. Phys. Rev. Lett. **95**, 052501 (2005). https://doi.org/10.1103/PhysRevLett.95.052501
103. D. Freire-Fernández, W. Korten, R.J. Chen, et al. Measurement of the isolated nuclear two-photon decay in ^{72}Ge. arXiv:2312.11313 [nucl-ex]
104. B. Sun, R. Knöbel, N. Kuzminchuk et al., A new resonator Schottky pick-up for short-lived nuclear investigations. GSI Sci. Rep. **2010**, 163 (2011)
105. X.L. Tu, X.C. Chen, J.T. Zhang et al., First application of combined isochronous and Schottky mass spectrometry: Half-lives of fully ionized $^{49}Cr^{24+}$ and $^{53}Fe^{26+}$ atoms. Phys. Rev. C **97**, 014321 (2018). https://doi.org/10.1103/PhysRevC.97.014321
106. A. Akber, M.W. Reed, P.M. Walker et al., Increased isomeric lifetime of hydrogen-like ^{192m}Os. Phys. Rev. C **91**, 031301 (2015). https://doi.org/10.1103/PhysRevC.91.031301
107. K. Yokoi, K. Takahashi, M. Arnould, The production and survival of ^{205}Pb in stars, and the ^{205}Pb-^{205}TI s-process chronometry. Astron. Astrophys. **145**, 339–346 (1985)
108. R. Daudel, M. Jean, M. Lecoin, Sur la possibilité d'existence d'un type particulier de radioactivité phénomène de créatione. J. Phys. Radium **8**, 238–243 (1947). https://doi.org/10.1051/jphysrad:0194700808023800
109. J.N. Bahcall, Theory of bound-state beta decay. Phys. Rev. **124**, 495–499 (1961). https://doi.org/10.1103/PhysRev.124.495
110. F. Bosch, T. Faestermann, J. Friese et al., Observation of bound-state β^- decay of fully ionized ^{187}Re: ^{187}Re–^{187}Os cosmochronometry. Phys. Rev. Lett. **77**, 5190–5193 (1996). https://doi.org/10.1103/PhysRevLett.77.5190
111. C. Brandau, C. Kozhuharov, A. Müller et al., Probing nuclear properties by resonant atomic collisions between electrons and ions. Phys. Scr. **T156**, 014050 (2013). https://doi.org/10.1088/0031-8949/2013/t156/014050
112. C. Brandau, C. Kozhuharov, in *Storage-Ring Studies of Dielectronic Recombination as a Tool for Precision Spectroscopy*. ed. by V. Shevelko, H. Tawara (Springer, Berlin, Heidelberg, 2012), pp.283–306
113. F. Bosch, S. Hagmann, P.-M. Hillenbrand et al., Search for bound-state electron+positron pair decay. EPJ Web Conf. **123**, 04003 (2016). https://doi.org/10.1051/epjconf/201612304003

114. V.I. Goldanskii, V.A. Namiot, On the excitation of isomeric nuclear levels by laser radiation through inverse internal electron conversion. Phys. Lett. B **62**, 393–394 (1976). https://doi.org/10.1016/0370-2693(76)90665-1
115. C.J. Chiara, J.J. Carroll, M.P. Carpenter et al., Isomer depletion as experimental evidence of nuclear excitation by electron capture. Nature **554**, 216–218 (2018). https://doi.org/10.1038/nature25483
116. Y. Wu, C.H. Keitel, A. Pálffy, ^{93m}Mo isomer depletion via beam-based nuclear excitation by electron capture. Phys. Rev. Lett. **122**, 212501 (2019). https://doi.org/10.1103/PhysRevLett.122.212501
117. S. Guo, B. Ding, X.H. Zhou et al., Probing ^{93m}Mo isomer depletion with an isomer beam. Phys. Rev. Lett. **128**, 242502 (2022). https://doi.org/10.1103/PhysRevLett.128.242502
118. A. Palffy, Z. Harman, C. Kozhuharov et al., Nuclear excitation by electron capture followed by fast x-ray emission. Phys. Lett. B **661**, 330–334 (2008). https://doi.org/10.1016/j.physletb.2008.02.027
119. J. Gunst, Y.A. Litvinov, C.H. Keitel, A. Pálffy, Dominant secondary nuclear photoexcitation with the X-ray free-electron laser. Phys. Rev. Lett. **112**, 082501 (2014). https://doi.org/10.1103/PhysRevLett.112.082501
120. L. Varga, et al. Phys. Rev. (2024) (submitted)
121. C.G. Bruno, J.J. Marsh, T. Davinson et al., CARME—the CRYRING array for reaction measurements: a new approach to study nuclear reactions using storage rings. Nucl. Instrum. Methods A **1048**, 168007 (2023). https://doi.org/10.1016/j.nima.2022.168007
122. P.G. Thirolf, S. Kraemer, D. Moritz et al., The thorium isomer ^{229m}Th: review of status and perspectives after more than 50 years of research. Eur. Phys. J. Spec. Top. (2024). https://doi.org/10.1140/epjs/s11734-024-01098-2
123. V.M. Shabaev, D.A. Glazov, A.M. Ryzhkov et al., Ground-state g factor of highly charged ^{229}Th ions: an access to the M1 transition probability between the isomeric and ground nuclear states. Phys. Rev. Lett. **128**, 043001 (2022). https://doi.org/10.1103/PhysRevLett.128.043001
124. Y.A. Litvinov, J. Glorius, T. Stöhlker et al., Precision experiments with heavy-ion storage rings. Acta Phys. Polon. B **16**, 4–25 (2023). https://doi.org/10.5506/APhysPolBSupp.16.4-A25
125. X. Zhou, J. Yang, Status of the high-intensity heavy-ion accelerator facility in China. AAPPS Bull. **32**, 35 (2022). https://doi.org/10.1007/s43673-022-00064-1
126. T. Stöhlker, Y.A. Litvinov, A. Bräuning-Demian, SPARC collaboration: new strategy for storage ring physics at FAIR. Hyperfine Interact. **227**, 45–53 (2014). https://doi.org/10.1007/s10751-014-1047-2
127. M. Durante, P. Indelicato, B. Jonson et al., All the fun of the FAIR: fundamental physics at the facility for antiproton and ion research. Phys. Scr. **94**, 033001 (2019). https://doi.org/10.1088/1402-4896/aaf93f
128. M. Grieser, Y.A. Litvinov, R. Raabe et al., Storage ring at HIE-ISOLDE. Eur. Phys. J. Spec. Top. **207**, 1–117 (2012). https://doi.org/10.1140/epjst/e2012-01599-9
129. The Nuclear Physics European Collaboration Committee, Expert Committee of the European Science Foundation. https://www.nupecc.org
130. R. Reifarth, Y.A. Litvinov, Measurements of neutron-induced reactions in inverse kinematics. Phys. Rev. ST Accel. Beams **17**, 014701 (2014). https://doi.org/10.1103/PhysRevSTAB.17.014701
131. R. Reifarth, K. Göbel, T. Heftrich et al., Spallation-based neutron target for direct studies of neutron-induced reactions in inverse kinematics. Phys. Rev. Accel. Beams **20**, 044701 (2017). https://doi.org/10.1103/PhysRevAccelBeams.20.044701
132. X. Xu, J. Liu, C. Yuan et al., Masses of ground and isomeric states of ^{101}In and configuration-dependent shell evolution in odd-A indium isotopes. Phys. Rev. C **100**, 051303(R) (2019). 10.1103/PhysRevC.100.051303